

Simple model of liquid-liquid phase transitions

H. K. Lee* and R. H. Swendsen

Department of Physics, Carnegie Mellon University, Pittsburgh, Pennsylvania 15213

(Received 8 June 2001; published 7 November 2001)

In recent years, a second fluid-fluid phase transition has been reported in several materials at pressures far above the usual liquid-gas phase transition. In this paper, we introduce a model of this behavior based on the Lennard-Jones interaction with a modification to mimic the different kinds of short-range orientational order in complex materials. We have done Monte Carlo studies of this model that clearly demonstrate the existence of a second first-order fluid-fluid phase transition between high- and low-density liquid phases.

DOI: 10.1103/PhysRevB.64.214102

PACS number(s): 64.70.Ja

The most common example of a first-order phase transition is that between a liquid and a gas, such as boiling water. On the other hand, while many transitions between different solid phases of homogeneous materials are also well known, it is only relatively recently that evidence of a second fluid-fluid phase transition has been found. In fact, liquid-liquid phase transitions (LLPT) have been suggested in liquid S, Ga, Se, Te, I₂, Cs, and Bi.¹

Stell and Hemmer^{2,3} showed the existence of LLPT in a one-dimensional model with a softened hard core potential and a long-range negative attraction. Their work was later studied in more detail by Franzese *et al.*⁴ and Sadr-Lahijany *et al.*⁵

Mitus, Patashinskii, and Shumilo⁶ proposed LLPT in molten salt at high pressure based on a phenomenological model. Ferraz and March suggested a similar LLPT in carbon, with indirect experimental evidence being found by Togaya.⁷ Glosli and Ree⁸ published results of a first-order liquid-liquid phase transition in molten Carbon between two thermodynamically stable liquid phases. Extensive computer simulations on models of water have supported the existence of a LLPT in the metastable region.⁹⁻¹⁶ Experimental results supporting the evidence of liquid-liquid phase transitions in water have also been found.¹⁷⁻¹⁹ Katayama and Mizutani *et al.*²⁰ found a liquid-liquid phase transition in molten phosphorus using x-ray diffraction.

Our objective is to investigate the general phenomenon instead of studying LLPT for any particular substance. We have developed a simple model that exhibits a transition between high- and low-density liquids at high pressure. The behavior of our model is constructed to be similar to behavior seen in simulations of real substances such as water and carbon but without introducing the complexity of having to simulate molecular orientations as in water and carbon.

To mimic the effects of local ordering, we have represented the different relative local orientations of the molecules with a spin-one-half variable. The interactions between particles with the same spin are given by the original Lennard-Jones expression, while the interactions between particles with opposite spin are purely repulsive:

$$\phi_{\uparrow\uparrow}(r) = \phi_{\downarrow\downarrow}(r) = 4\epsilon \left(\frac{\sigma_l^{12}}{r^{12}} - \frac{\sigma_l^6}{r^6} \right), \quad (1)$$

$$\phi_{\uparrow\downarrow}(r) = \phi_{\downarrow\uparrow}(r) = 4\epsilon \left(\frac{\sigma_u^{12}}{r^{12}} \right). \quad (2)$$

Note that there are different values of σ for like and unlike spins. This is an important feature of the model, and some properties, including the symmetries of the solid phases, are sensitive to the relative values of σ_l and σ_u . The LLPT occurs when σ_u is smaller than σ_l , so that by reorienting the spins, the particles are capable of forming different coordination numbers and local structures. We have performed most of our investigations for the case in which the ratio is 1/2.

Our model can be modified to couple to a fictitious external magnetic field. If we define the magnetic moment as the sum of all spins, then the Hamiltonian is given by

$$H = \frac{1}{2} \sum_{i \neq j} \phi_{ij}(r_{ij}) - h \sum_i \sigma_i. \quad (3)$$

h is the fictitious magnetic field which is set to zero in our simulations and $\sigma_i = \pm 1$ is the direction of the spins of individual particles. We used the units $T^* = k_B T / \epsilon$, $P^* = \sigma_l^2 k_B P / \epsilon$. We have set the potential cutoffs at $3\sigma_l$.

We performed Monte Carlo simulations of the two-dimensional version of our model in various ensembles. Although our simulations are done in two dimensions, our model is not limited to two dimensions. The simulations turned out to be rather difficult, and it was necessary to extend the usual techniques to improve efficiency. However, we did find clear evidence of an LLPT at high pressures. We are able to map out both PT and P ρ phase diagrams.

For our simulations of fluids, we confined the particles to a square with periodic boundary conditions. For those simulations that were extended to include solid phases, we used parallelograms to allow us to vary the angle of the boundary conditions, as well as the volume of the container. Simulation step sizes for individual particle motion, changes of the volume of the box, and changes of the angle of the parallelogram were dynamically optimized using the acceptance ratio method.²¹ Metropolis flips to maintain equilibrium for the spins associated with each particle were also carried out.

Volume changes on the dense fluid turned out to be rather inefficient because $\phi_{\uparrow\downarrow}$ increases very rapidly at short distances. We solved this problem by introducing a cluster

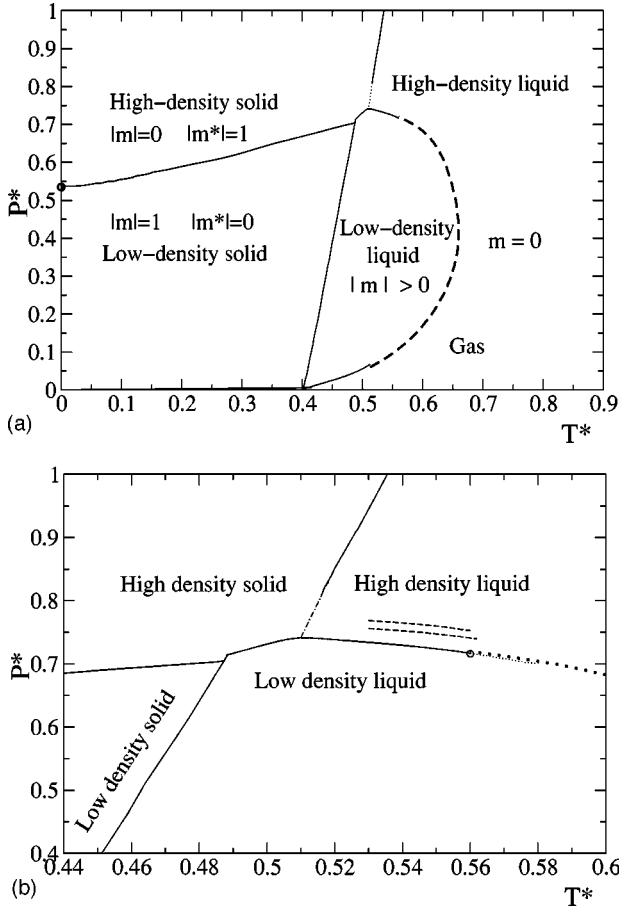


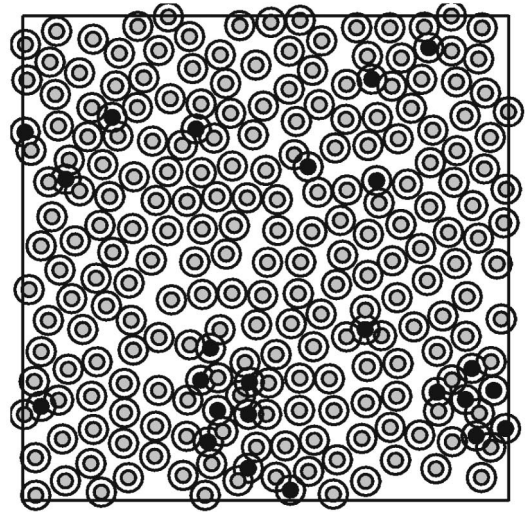
FIG. 1. (a) PT diagram. Solid lines show coexistence curves obtained from our simulations with 160 particles. \circ marks the calculated solid-solid transition point at $T=0$. Dotted lines show our estimate for the coexistence curves. The thick dashed line represents the locus of Curie points for the second-order magnetic transitions. $|m|$ and $|m^*|$ are the magnetic and antimagnetic order parameters, respectively. (b) PT diagram in the region of interest, the circle marks the tricritical point and dotted line shows the peak of the isothermal compressibility beyond tricritical point. Solid lines show coexistence curves obtained from our simulations with 160 particles. The dashed line shows the extent of curve shifting due to the finite size effect. The upper dashed line corresponds to a system with 480 particles and the lower dashed line corresponds to a system with 320 particles.

Monte Carlo move. The clusters are formed by creating bonds between particles with probability

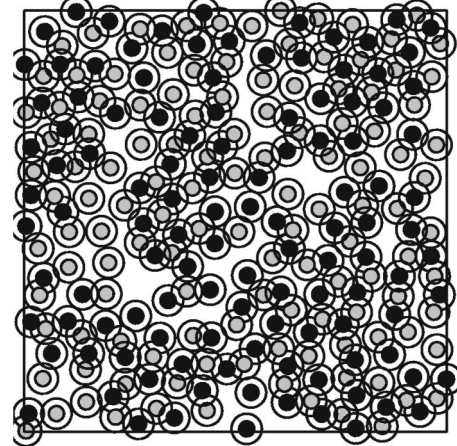
$$P(r) = \begin{cases} 1, & r < r_{\min}, \\ (r_{\max} - r)/(r_{\max} - r_{\min}), & r \in [r_{\min}, r_{\max}], \\ 0, & \text{otherwise} \end{cases} \quad (4)$$

and then changing the size of the box by rescaling the locations of the centers of mass of the clusters. This cluster move is extremely effective, with $r_{\min} = 0.675\sigma_l$ and $r_{\max} = 0.725\sigma_l$, we achieved improvements in the acceptance ratio by factors of up to 10^{10} .

The probability of accepting a proposed cluster move is given as follows. Let \mathcal{E} be the set of all edges that join any



(a)



(b)

FIG. 2. Snapshots of a system of 240 particles in the low-density (a) and high-density (b) liquid state coexisting at $T^* = 0.55$, $P^* = 0.75$, $\rho^* = 0.833$, and 1.25 , respectively.

two particles which are less than $3\sigma_l$ apart, and let \mathcal{B} be the subset of \mathcal{E} consisting of bonds formed with the probability $P(r)$, where r is the edge length joining the two particles. Let the edges, bonds and edge lengths of the new configuration be denoted by \mathcal{E}' , \mathcal{B}' , and r' , respectively. The probability of forming \mathcal{B} is

$$P(\mathcal{B}) = \prod_{i \in \mathcal{B}} P(r_i) \prod_{j \in \mathcal{E} - \mathcal{B}} 1 - P(r_j). \quad (5)$$

Bond configurations need to remain invariant in order to satisfy detailed balance. Therefore $\mathcal{B} = \mathcal{B}'$, $r_i = r'_i$ for all $r_i \in \mathcal{B}$ and $r'_i \in \mathcal{B}'$, but $r_j \neq r'_j$ for $r_j \in \mathcal{E} - \mathcal{B}$ and $r'_j \in \mathcal{E}' - \mathcal{B}'$. Therefore,

$$\prod_{i \in \mathcal{B}} P(r_i) / \prod_{i' \in \mathcal{B}'} P(r'_i) = 1 \quad (6)$$

and

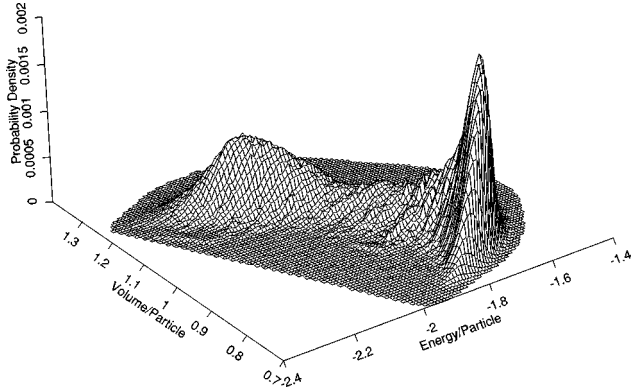


FIG. 3. Probability density function for 240 particles coexisting at $T^*=0.54$ and $P^*=0.75$.

$$\frac{P(B')}{P(B)} = \frac{\prod_{j' \in \mathcal{E}'-B'} [1-P(r_{j'})]}{\prod_{j \in \mathcal{E}-B} [1-P(r_j)]}. \quad (7)$$

Hence the acceptance probability is

$$A(\varpi \rightarrow \varpi') = \min \left(1, e^{-\beta(\Delta E + p\Delta V)} \frac{V'^N \prod_{i \in \mathcal{E}'-B'} [1-P(r_i)]}{V^N \prod_{i \in \mathcal{E}-B} [1-P(r_i)]} \right). \quad (8)$$

Another new move that has proven extremely effective is to form clusters of nearby particles that are less than $1/\sqrt{\rho} \sin(\pi/3)$ apart and attempt to flip the spins of all particles in a cluster.

For canonical ensemble simulations using two boxes in equilibrium with each other, the total volume is conserved.²³ An additional Monte Carlo move is introduced to transfer particles between the boxes.

Thermodynamic quantities were calculated from simulations in the constant pressure ensemble over relatively large

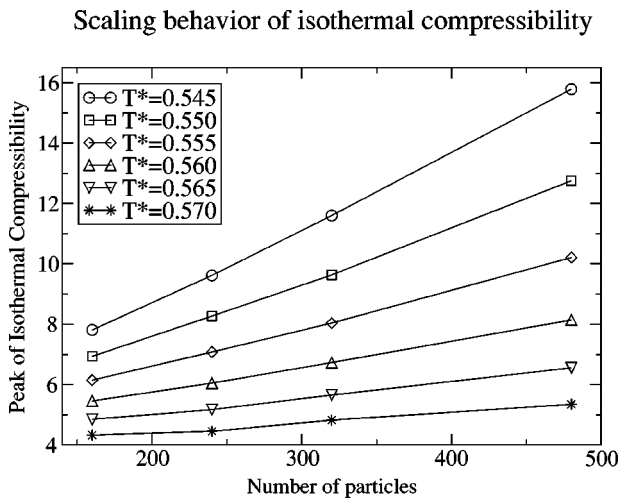


FIG. 4. Plot of peak values of isothermal compressibility vs system size. The tricritical point is near $T^*=0.56$.

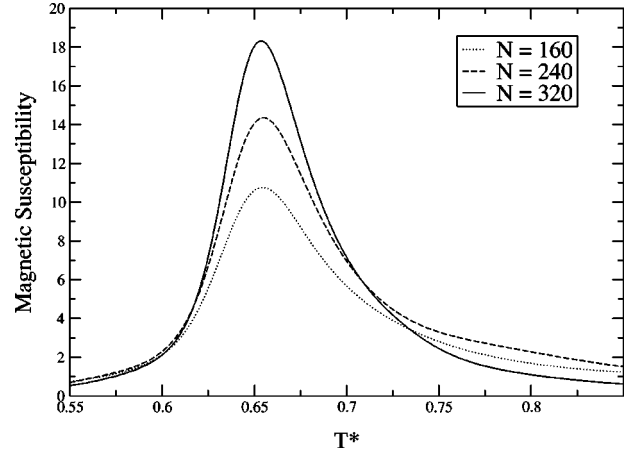


FIG. 5. Magnetic susceptibility plotted against T^* at $P^*=0.5$ and $h=0$.

pressure and temperature domains using the multiple histogram method.²² The coexistence curve is mapped out by tracing the ridge line of the isothermal compressibility. The position of the tricritical point was estimated using finite size scaling. The $P\rho$ diagram was determined by combining other data with the results of simulations using the canonical ensemble.²³

The phase diagram for our model is shown in Fig. 1. At low pressures its behavior is virtually identical to that of the usual Lennard-Jones model. At higher pressures, the coexistence curve for the LLPT is shown projecting into the fluid region of the phase diagram. This line of first-order phase transitions actually ends in a tricritical point, which separates it from a locus of critical points associated with the ordering of the “spins” used to define the model. This locus of critical points joins the liquid-gas and liquid-liquid first-order coexistence curves at the tricritical points. However, it is only our access to the “magnetic” degrees of freedom in the model

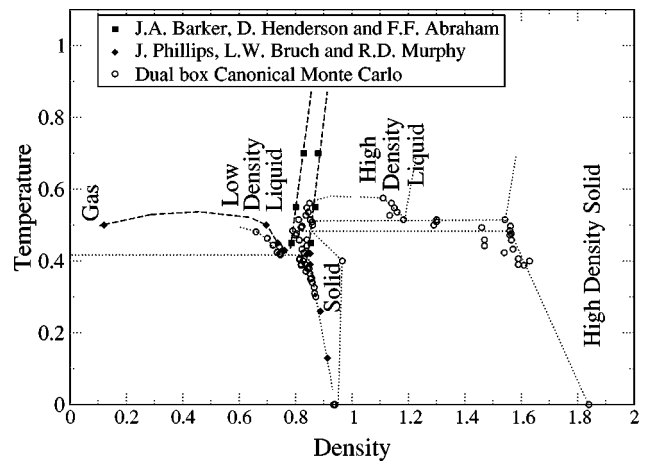


FIG. 6. ρ - T diagram. Points obtained by simulation using the canonical ensemble with 160 particles in two boxes. Dashed lines show the coexistence region of the pure Lennard-Jones system reported by Barker, Henderson, and Abraham and Phillips, Bruch, and Murphy. Dotted lines show the coexistence region of our model. All lines are drawn to guide the eye.

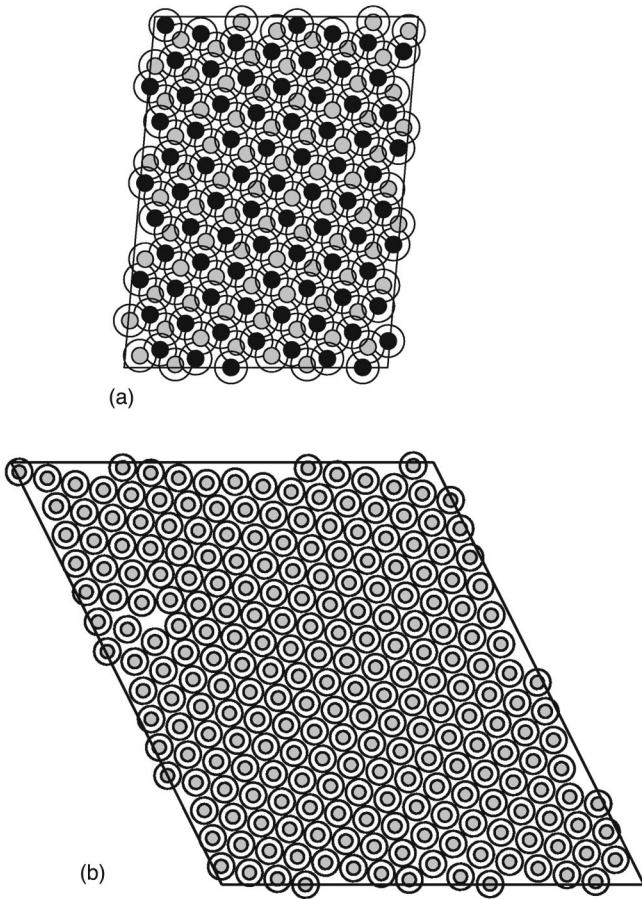


FIG. 7. The high-density (a) and low-density (b) solid states, notice a vacancy in the low-density solid state.

that make it obvious that the LLPT curves end in tricritical rather than critical points. If we did not have access to the magnetic degrees of freedom, rather careful measurement of the exponents characterizing the divergences at the end of the line of first-order transitions would be necessary to distinguish the two cases. It is not completely clear whether a fictitious ordering field in a more elaborate model would not have the same consequence of producing tricritical points.

The apparent discontinuity of the coexistence curves between the high-density solid, the low-density solid and the low-density liquid is an artifact of the accuracy of our simulations. These lines are obtained from the multiple histogram extrapolations in opposite directions. The fact that these two lines do not meet exactly, but terminated very close to each other shows the accuracy of our simulations.

To determine the liquid-liquid coexistence curve in the PT diagram, simulations were done with 160 particles at constant pressure, using larger systems to check the results. Sets of histograms were collected at $T^* = 0.53, 0.55, \text{ and } 0.565$ over a range of pressures covering across the coexistence region. The system was equilibrated for 30 000 MCS/P before beginning to take data for another 300 000 MCS/P.

To determine the tricritical point for the liquid-liquid phase transition, additional simulations for 160, 240, 320, and 480 particles were done at constant pressures at $T^* = 0.55$ and 0.565 . The Monte Carlo simulations used a total

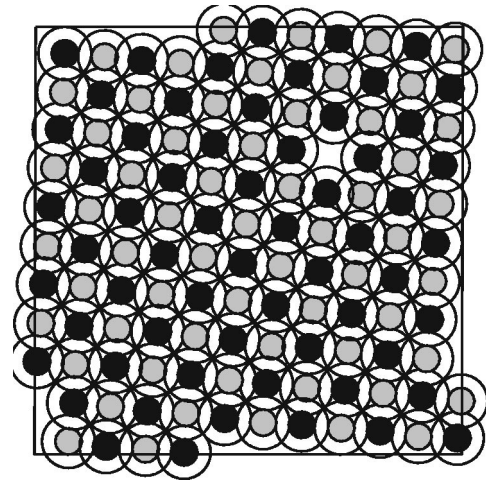


FIG. 8. Fourfold solids form using a model with $\tau = 0.6$.

of 300 000 MCS/P for the 160 particle systems and typical equilibration runs of 30 000 MCS/P. For larger systems, longer runs were used. For the 480 particle system, a total of 1 200 000 MCS/P were used with typical equilibration runs of 100 000 MCS/P.

To determine the liquid-solid coexistence curve, simulations were performed at $P^* = 0.5, 0.6, 0.78, \text{ and } 0.9$ over a range of temperatures covering the solid-liquid coexistence region. The system was equilibrated for 60 000 steps per particle before collecting data for another 600 000 steps per particle.

The phase transition between high- and low-density phases is strongly first-order. Figures 2(a) and 2(b) show snapshots of high- and low-density liquids near the coexistence curve for a system with 240 particles. The low-density liquid is dominated by parallel nearest-neighbor interactions with a stronger core repulsion and with coordination number 6. The high-density liquid is dominated by an antiparallel nearest-neighbor interaction that allows the particles to come closer together and with coordination number 3. The differences in local orderings for low- and high-density liquids stabilize the liquids and create the possibility of liquid-liquid phase transitions.

The volume-energy probability density function (Fig. 3) has a saddle point that is typical of a first-order transition. The coexistence curve for the LLPT has a negative slope, as shown in the PT diagram in Fig. 1, reflecting the higher entropy of the high-density liquid. The sharp bend of the liquid-solid coexistence curve at the triple point found from the multiple-histogram analysis is consistent with our observation of the liquid-liquid phase transition.

To find the tricritical point, we use the fact that peak values of the isothermal compressibility grow as $\mathcal{O}(N)$ at the coexistence curve and as $\mathcal{O}(N^{0.925})$ (Refs. 24–29) at the tricritical point, assuming that the transition is in the expected two-dimensional Ising class. Simulations were done with $N = 160, 240, 320, \text{ and } 480$ near the tricritical point. Peak values of the isothermal compressibility are then plotted against system sizes for various temperatures. Figure 4 shows the size dependence of the isothermal compressibility. Although

it is hard to determine the exact location of the tricritical point, the data suggest that it is located at $T^* = 0.56 \pm 0.01$.

Figure 5 shows the growing divergence of the magnetic susceptibility for 160, 240 and 320 particles. These magnetic susceptibility are plotted at $P^* = 0.5$ which is far away from the liquid-liquid coexistence curve and the gas-liquid coexistence curve.

The ρ - T diagram (Fig. 6) was mapped out using simulations in the canonical ensemble using dual boxes to simulate coexistence without the inconvenience of an interface between the phases.²³ The low-density liquid-gas coexistence region is only slightly lower than that of pure Lennard-Jones^{30,31} due to the small effect of the differences in the models at low densities.

Figure 7(a) shows a snapshot of the high-density crystalline state, which has threefold symmetry and zero magnetic moment. The low-density crystalline state [Fig. 7(b)] is hexagonal close packed with uniform spin. At zero temperature, we can calculate the location of the transition between the two solid phases to arbitrary precision. Its location is determined to be $P^* = 0.534819 \pm 10^{-7}$, with $\rho^* = 1.82646$ and $\rho^* = 0.943122$ for the high- and low-density solids, respectively. For comparison, $\rho^* = 0.934721$ at $T^* = 0$ and $P^* = 0$, so the low-density solid phase changes its density very little up to the boundary of the high-density phase.

It was found that symmetry of the solid phase is highly

dependent on the ratio $\tau = \sigma_u / \sigma_l$. Figure 8 shows a solid with fourfold symmetry obtained from a simulation with $\tau = 0.6$. We believe that the full range of solid phases is quite rich for this model.

We have developed a relatively simple model that demonstrates a liquid-liquid phase transition between high- and low-density phases. Although our simulations are two dimensional, our model is not restricted to two dimensions and we see no reason to believe that a three-dimensional simulation with our model would produce significantly different behavior. By comparing the behavior of our model with the properties of real systems, we hope to learn which properties are generic and which depend on details of a particular material. One immediate point of interest is the negative slope of the liquid-liquid coexistence line in our model, which reflects the high entropy in the high-density phase. This feature is, indeed, found in most materials that exhibit an LLPT. However, this does not appear to be universal, since the coexistence curve of molten carbon reported by Glosli and Ree⁸ has a positive slope. At the present time, this difference in materials properties is not understood.

We would like to thank Professor Robert Griffiths for his suggestions and helpful comments. We also would like to acknowledge the support from the Pittsburgh Supercomputing Center.

*Current address: Dept. of Physics, University of Georgia, Athens, GA 30602, U.S.A.; Computer Science and Mathematics Department, Oak Ridge National Laboratory, Bldg 6012, Bethel Valley Road, Oak Ridge, TN 37831-6367.

¹A. Ferraz and N.H. March, Phys. Chem. Liq. **8**, 289 (1979).

²G. Stell and P.C. Hemmer, J. Chem. Phys. **56**, 4274 (1972).

³P.C. Hemmer and G. Stell, Phys. Rev. Lett. **24**, 1284 (1970).

⁴G. Franzese, G. Malescio, A. Skibinsky, S.V. Buldyrev, and H.E. Stanley, Nature (London) **409**, 692 (2001).

⁵M.R. Sadr-Lahijany, A. Scala, and S.V. Buldyrev, H.E. Stanley, Phys. Rev. Lett. **81**, 4895 (1998).

⁶A.C. Mitus, A.Z. Patashinskii, and B.I. Shumilo, Phys. Lett. **113A**, 41 (1985).

⁷M. Togaya, Phys. Rev. Lett. **79**, 2474 (1997).

⁸J.N. Glosli and F.H. Ree, Phys. Rev. Lett. **82**, 4659 (1999).

⁹M. Meyer and H.E. Stanley, J. Phys. Chem. B **103**, 9728 (1999).

¹⁰H.E. Stanley, L. Cruz, S.T. Harrington, P.H. Poole, S. Sastry, F. Sciortino, F.W. Starr, and R. Zhang, Physica A **236**, 19 (1997).

¹¹S. Harrington, R. Zhang, P.H. Poole, F. Sciortino, and H.E. Stanley, Phys. Rev. Lett. **78**, 2409 (1997).

¹²S. Harrington, P.H. Poole, F. Sciortino, and H.E. Stanley, J. Chem. Phys. **107**, 7443 (1997).

¹³P.H. Poole, U. Essmann, F. Sciortino, and H.E. Stanley, Phys. Rev. E **48**, 4605 (1993).

¹⁴P.H. Poole, F. Sciortino, U. Essmann, and H.E. Stanley, Nature (London) **360**, 324 (1992).

¹⁵H. Tanaka, Phys. Rev. Lett. **80**, 113 (1998).

¹⁶E. Shiratani and M. Sasai, J. Chem. Phys. **108**, 3264 (1998).

¹⁷O. Mishima, Phys. Rev. Lett. **85**, 334 (2000).

¹⁸A.K. Soper and M.A. Ricci, Phys. Rev. Lett. **84**, 2881 (2000).

¹⁹M.-C. Bellissent-Funel, Europhys. Lett. **42**, 161 (1998).

²⁰Y. Katayama, T. Mizutani, W. Utsumi, O. Shimomura, M. Yamakata, and K. Funakoshi, Nature (London) **403**, 170 (2000).

²¹D. Bouzida, S. Kumar, and R.H. Swendsen, Phys. Rev. A **45**, 8894 (1992).

²²A.M. Ferrenberg and R.H. Swendsen, Phys. Rev. Lett. **61**, 2635 (1988).

²³A.Z. Panagiotopoulos, Mol. Phys. **61**, 813 (1987).

²⁴M.P.M. den Nijs, J. Phys. A **12**, 1857 (1979).

²⁵B. Nienhuis, A.N. Berker, E.K. Riedel, and M. Schick, Phys. Rev. Lett. **43**, 737 (1979).

²⁶R.B. Pearson, Phys. Rev. B **22**, 2579 (1980).

²⁷B. Nienhuis, E.K. Riedel, and M. Schick, J. Phys. A **43**, 189 (1980).

²⁸M.P. M den Nijs, Phys. Rev. B **27**, 1674 (1983).

²⁹B. Nienhuis, J. Phys. A **15**, 199 (1982).

³⁰J.A. Barker, D. Henderson, and F.F. Abraham, Physica A **106**, 226 (1981).

³¹J.M. Phillips, L.W. Bruch, and R.D. Murphy, J. Chem. Phys. **75**, 5097 (1981).